particles

MDPI

Article

β Decay of ^{20}Na

Qiang Wang [1], You-Bao Wang [1,*], Jun Su [2,*], Zhi-Yu Han [1], B. Alex Brown [3], Li-Hua Chen [1], Zi-Qiang Chen [4], Bao-Qun Cui [1], Bo Dai [4], Tao Ge [1], Xin-Yue Li [1], Yun-Ju Li [1], Zhi-Hong Li [1], Gang Lian [1], Yin-Long Lyu [1], Rui-Gang Ma [1], Tian-Li Ma [1], Xie Ma [1], Ying-Jun Ma [1], Yi Su [1], Bing Tang [1,*], Chun-Guang Wang [4], Hong-Yi Wu [4], Fu-Rong Xu [4], Sheng-Quan Yan [1], Sheng Zeng [1], Hao Zhang [1], Yun Zheng [1], Chao Zhou [5], Yang-Ping Shen [1], Bing Guo [1,6], Tian-Jue Zhang [1] and Wei-Ping Liu [1,7]

1 China Institute of Atomic Energy, Beijing 102413, China
2 Key Laboratory of Beam Technology of Ministry of Education, School of Physics and Astronomy, Beijing Normal University, Beijing 100875, China
3 Facility for Rare Isotope Beams (FRIB), and Department of Physics and Astronomy, Michigan State University, East Lansing, MI 48824-1321, USA
4 School of Physics, Peking University, Beijing 100871, China
5 School of Nuclear Science and Technology, University of South China, Hengyang 421001, China
6 School of Physics, Xi'an Jiaotong University, Xi'an 710049, China
7 College of Science, Southern University of Science and Technology, Shenzhen 518055, China
* Correspondence: ybwang@ciae.ac.cn (Y.-B.W.); sujun@bnu.edu.cn (J.S.); tangb364@ciae.ac.cn (B.T.)

Abstract

^{20}Na is a well-known β-delayed α emitter, owing to the large decay energy of ^{20}Na above the α+^{16}O threshold in the $A = 5\alpha$ daughter nucleus ^{20}Ne. In this work, the decay property of ^{20}Na is investigated in detail via the β-γ β-α and β-γ-α coincidence spectroscopy. As the day-one experiment of the Beijing Rare Isotope Facility (BRIF), the intense ^{20}Na beam was produced using the Isotope Separator On Line (ISOL) technique through the 100 MeV proton bombarding a stack of MgO as a thick target. Specific interest was focused on the exotic decay mode of ^{20}Na; the previously reported low-energy α lines at 713 and 846 keV were confirmed, and several weak β-γ-α decay sequences were clearly identified for the first time, thanks to the strong resolving power of α-γ coincidence spectroscopy. The decay properties of ^{20}Na are compared to the shell model calculation, which agree reasonably well with the allowed β transition strengths and subsequent electro-magnetic transitions with the use of the sd shell-model space with the USDB interaction.

Keywords: ^{20}Na radioactivity; β-γ β-α and β-α-γ coincidence spectroscopy; exotic decay mode; B(F) and B(GT); Beijing Rare Isotope Facility (BRIF)

Check for updates

Academic Editor: Volodymyr Tretyak

Received: 27 February 2026
Revised: 25 March 2026
Accepted: 8 April 2026
Published: 17 April 2026

Copyright: © 2026 by the authors. Licensee MDPI, Basel, Switzerland. This article is an open access article distributed under the terms and conditions of the Creative Commons Attribution (CC BY) license.

1. Introduction

The Radioactive Ion Beam (RIB) facility has been one of the main focuses in nuclear physics for decades; it provides a powerful tool for exploring the nuclei in the domain of terra incognita and extending our knowledge obtained with stable beams [1]. About 270 stable and 50 long-lived nuclides are naturally occurring; they emerge as the remains of various stellar nucleosynthesis processes in different astrophysical scenarios. Numerous unstable isotopes are crucially involved in various high-temperature astrophysical processes; their decay properties and the reaction rates are indispensable inputs to the understanding of star evolution and explosive cosmic events [2,3]. Short-lived isotopes are crucial in nuclear physics for the exploration of the boundary of existence of nuclei; their

exotic structure [4,5] and abnormal reaction dynamics [6] bring a stringent challenge to theoretical models for a more complete description [7].

^{20}Na is a proton drip-line nucleus. It decays with a half-life of 447.9(23) ms and a decay energy of 13,892.5(11) keV [8,9] to the daughter nucleus ^{20}Ne. The spin and parity of the ground state of ^{20}Na is 2^+, and the isospin $T = 1$; its decay mainly proceeds through the allowed transitions to the 1^+, 2^+ and 3^+ states in ^{20}Ne with T = 0 or 1. Since the decay energy of ^{20}Na is well above the α threshold of ^{20}Ne ($S_\alpha = 4.730$ MeV), many α cluster states in ^{20}Ne can be populated in the decay of ^{20}Na with a total α-emission probability of about 20% [10]. The α resonance states in ^{20}Ne close to the threshold have been the focus in several works for the astrophysical Helium-burning reaction ^{16}O(α, γ)^{20}Ne [11–14]. For this purpose, the resonance width and the detailed γ transition strengths of ^{20}Ne α-cluster states are needed. ^{20}Na is also involved in the breaking of the hot CNO cycle reaction sequence: ^{15}O(α,γ)^{19}Ne (p,γ)^{20}Na(p,γ)^{21}Mg [15]. The β^+ decay of ^{20}Na competes with the ^{20}Na(p,γ)^{21}Mg reaction for NeNa cycle and the rapid proton capture process pathway.

According to the selection rule of allowed β transitions, the 1^+, 2^+ and 3^+ states in ^{20}Ne are directly populated in the ^{20}Na decay. However, only the ^{20}Ne resonance states with natural parity can decay directly to the ground state of ^{16}O; the high-lying 1^+ and 3^+ states in ^{20}Ne have to de-excite via γ rays for the sake of isospin conservation. An exotic β-γ-α decay mode may exist in ^{20}Na; i.e., the high-lying 1^+ and 3^+ states in ^{20}Ne may de-excite by γ rays to resonance states with natural parity and then emit α to the ground state of ^{16}O. A similar exotic β-γ-p decay mode was observed in ^{56}Zn [16] and ^{32}Ar [17], and it resulted in significant corrections to the β decay branching ratios and reduced transition strengths. These kinds of exotic decay modes become increasingly important for isotopes close to the proton drip line [18]; particle emission from unbound levels in the daughter nuclei may be partially or even totally due to the often omitted indirect feeding by γ transitions.

Many experimental investigations have been carried out concerning the decay of ^{20}Na since the 1960s. Macfarlane and Siivola first observed four groups of β-delayed α's from the ^{20}Na source produced by the charge-exchange reaction [19]. Pearson pointed out, in the same year, the probable existence of α groups lower than 1 MeV [20], which attracted several further investigations [15,21–25], but the low-energy α groups were not directly discovered. At the IGISOL facility, Laursen et al. conducted a high-statistics measurement of the β-delayed α spectrum of ^{20}Na [26]. By applying the α and ^{16}O coincidence, two groups of α's below 1 MeV were successfully observed, and they were assigned to the known 3^- state at 5621 keV and the 1^- state at 5788 keV in ^{20}Ne, respectively. Based on these new α particle lines, exotic β-γ-α sequences were suggested, including the one from the IAS at 10,277 keV to the 5621 keV 3^- state in ^{20}Ne [26]. It is interesting to notice that the previous measurements are mostly β-delayed single-α or single-γ measurements. With the purpose of directly exploring the exotic decay sequences of ^{20}Na, we conducted this measurement with β-delayed α-γ coincidence spectroscopy. Some of the results concerning the direct observation of the exotic β-γ-α decay sequences in ^{20}Na have been published as a letter in Ref. [27].

2. Experiment

2.1. Beam Production

The Beijing Rare Isotope Facility (BRIF) [28,29] is an ISOL-type radioactive ion beam facility that is an upgrade project aiming to provide post-accelerated beams of rare isotopes at the Beijing HI-13 heavy-ion Tandem accelerator laboratory [30]. At BRIF, radioactive nuclides are produced by a proton beam of 100 MeV bombarding a thick target; the reaction products that diffuse out of the target are ionized by an ion source and separated by a

high-resolution Isotope Separator On Line (ISOL) for subsequent post-acceleration in the HI-13 Tandem accelerator. The driving accelerator of BRIF is a home-made 100 MeV, 500 μ A proton cyclotron (CYCIAE-100) equipped with a fixed field and four sectors. CYCIAE-100 adopts a compact magnet of 6.16 m in diameter with a pole radius of 2.0 m and H^- acceleration with stripping extraction [31]. The ISOL part of BRIF consists of pre-separation and main separation stages that employ different potentials [32]. The pre-separation stage, with $M/\Delta M = 2000$, includes two 90° bending magnets and electrostatic quadrupoles placed on a 300 kV platform, which keeps the unwanted radioactivities at the heavily shielded front end; the main separation stage, with $M/\Delta M = 20{,}000$, is energy-achromatically fulfilled with two large 100° bending magnets. BRIF is capable of delivering low-energy ISOL beams of 60–300 keV and post-accelerated beams from 3 to 10 MeV/u for nuclei with mass numbers of A < 80. Two types of ion sources are equipped at BRIF [33]; one is a surface ion source for low-ionization-potential elements, and the other is an electron-impact ion source for gaseous and high-ionization-potential elements. Since the mass resolution of the pre-separation stage was sufficient for the present experiment, a conventional reaction chamber was installed at the entrance of the main separation magnet, and electrostatic quadruples at the front end were adjusted to focus the ISOL beam on the center of the target chamber.

In this day-one experiment, the ^{20}Na source was produced by the ^{24}Mg$(p,\alpha n)^{20}$Na reaction with a 100 MeV proton beam bombarding a MgO target. The MgO target is about 10 cm thick, comprising a stack of MgO slices, each with a thickness of about 2 mm. To facilitate the effusion of neutral ^{20}Na atoms out of their production lattices, each MgO slice was made into a microporous structure, and 1/4 of each slice was deliberately cut off to form a diffusion volume in the target oven of a cylindric tantalum tube. The MgO target material has a melting temperature of 2852 °C and the operating temperature was optimized to about 1500 °C in the experiment [33]. Four experiments were carried out in a period of one year for the production of an intense ^{20}Na ISOL beam. Steady progress was achieved, owing to the growing knowledge of the optimum working condition of the target-ion source system [33]. A ^{20}Na intensity of 1×10^5 pps was reached ultimately with a 5 μ A proton primary beam, resulting in an overall efficiency of about 0.01%, which is comparable to the result reported from a TRIUMF-ISAC experiment [34]. Moreover, ISOL beams of $^{21,22,24-26}$Na isotopes were also produced with the thick MgO target; the intensity of ^{21}Na ($t_{1/2} = 22.49$ s) was at least three orders of magnitude higher than that of ^{20}Na under the same condition, which was later post-accelerated for a nuclear reaction study [35].

2.2. Experimental Setup

The experimental setup for the β decay of ^{20}Na is shown in Figure 1. A pure beam of ^{20}Na 1^+ ions at 100 keV was implanted into a 3 μ m-thick aluminum collection foil. The aluminum foil is positioned at the geometric center of a silicon box, which consists of five 1 mm-thick multiguard silicon quadrant (MSQ) detectors for the measurement of β particles from the ^{20}Na decay. The performance of the MSQ detectors was checked with a ^{133}Ba source. The thickness of the aluminum collection foil allows the strongest β-delayed α particle group of ^{20}Na, at 2.15 MeV, to go through and be measured by an MSQ detector. Two double-sided silicon strip detectors (DSSDs) are symmetrically installed at backward angles relative to the beam axis, each at a linear distance of 10 cm from the aluminum foil. The DSSDs have an active thickness of approximately 70 μ m and a very thin dead layer of only 100 nm for the efficient detection of low-energy α particles. An MSQ detector of 1 mm in thickness is mounted behind each DSSD to veto β-particles and remove the β-α summing events. Standard α sources of ^{239}Pu and ^{241}Am were used to check the performance of the

DSSDs and the MSQ detectors before and after the experiment. Two HPGe detectors, each with a relative efficiency of 175%, are placed in two cylindric flanges perpendicular to the beam direction to measure the β-delayed γ rays from ^{20}Na. The flange has a very thin front wall of only 1 mm to avoid the absorption of low-energy γ rays from ^{20}Na.

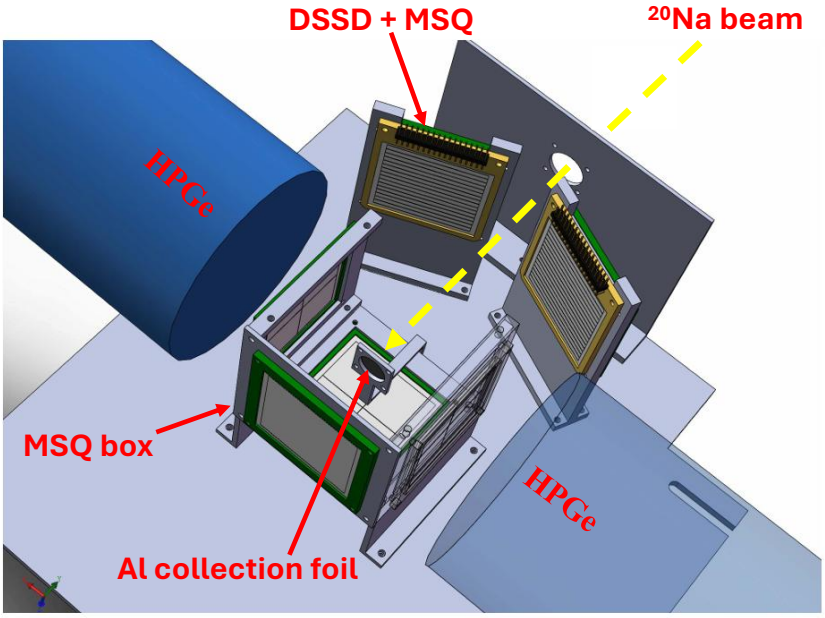


Figure 1. Experimental setup for the β decay of ^{20}Na. The top MSQ has been removed to show the inner geometry and the collection foil that is tilted into the center of the MSQ box from the upstream.

The energy signals from the MSQ, DSSD, and HPGe detectors are acquired by a 12-bit analog-to-digital converter CAEN V785 (Italy), while the timing signals are recorded by a time-to-digital converter, CAEN V1190 (Italy), with a time resolution set to 100 ps. The MSQ detectors work at a bias voltage of −100 V supplied by a Mesytec (Germany) MHV-4 high-voltage module. Their output signals are processed by a Mesytec (Germany) 8-channel integrated preamplifier and the main amplifier before being fed into the V785. The two HPGe detectors are biased at +2400 V and +3400 V, respectively, using an ORTEC (USA) 660 high-voltage power supply. Their signals are shaped by ORTEC (USA) 672 amplifiers and then sent to the V785. The two DSSDs are operated at a bias voltage of −6 V. Their signals are processed by a Mesytec 16-channel integrated preamplifier and main amplifier before being fed into the V785. The data acquisition system was triggered by a β particle signal from the MSQ detectors, with a width of 32 μ s to accommodate the α from the DSSDs and γ from the HPGe detectors. During the period of the experiment, the implantation rate of ^{20}Na was controlled to an average of about 1.5×10^4 pps. With this implantation rate, the average live time of the data acquisition system was about 75%, and about 4.5×10^9 ^{20}Na nuclei in total were implanted into the collection foil.

The relative efficiency of the HPGe detector was calibrated using the 1779, 3454, and 5110 keV γ rays from the well-known resonant reaction ^{27}Al$(p,\gamma)^{28}$Si at $E_p = 293$ keV [36], as shown in Figure 2. Measurements were obtained at source-to-detector distances ranging from 4 to 35 cm. These data were used to constrain the Geant4 simulation for the optimum HPGe detector model. The absolute detection efficiency of the HPGe detectors was identified by a Geant4 simulation for γ rays of up to 12 MeV under the realistic experimental conditions of this work, as shown in Figure 3. The summing effect caused by the close detector geometry was automatically taken into account when the Geant4 simulation was performed to reproduce the γ spectra from the standard sources and the ^{27}Al$(p,\gamma)^{28}$Si

reaction. The HPGe detector efficiency data obtained from the Geant4 simulations were fitted using the following function:

$$\varepsilon(E) = a \exp\left(b + cE + d \ln E + e \ln^2 E\right) \quad (1)$$

Two sets of fitting parameters were obtained for the two HPGe detectors, respectively:

$$a_0 = 0.6224,\ b_0 = 0.5056,\ c_0 = -0.07428,\ d_0 = -0.4084,\ e_0 = -0.02543;$$

$$a_1 = 0.06915,\ b_1 = 0.5112,\ c_1 = -0.0804,\ d_1 = -0.3988,\ e_1 = -0.01852.$$

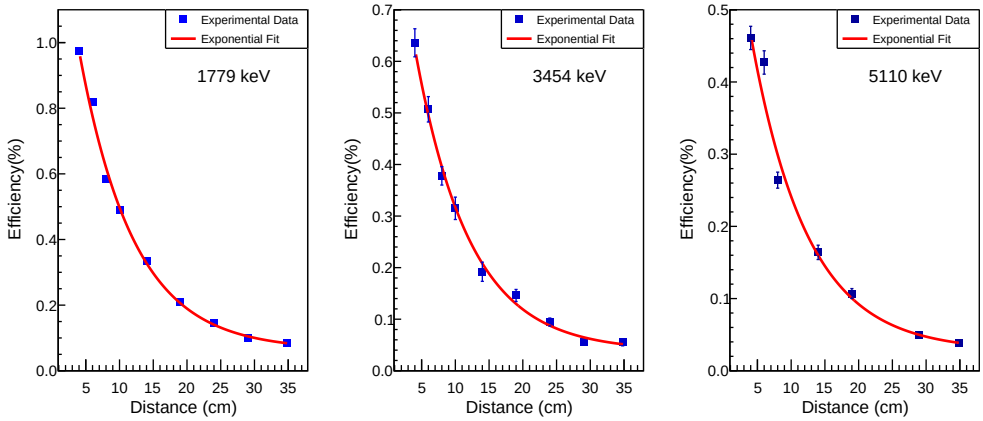


Figure 2. The relative detection efficiency of the HPGe detector calibrated by the γ rays from the ^{27}Al$(p,\gamma)^{28}$Si reaction at $E_p = 293$ keV.

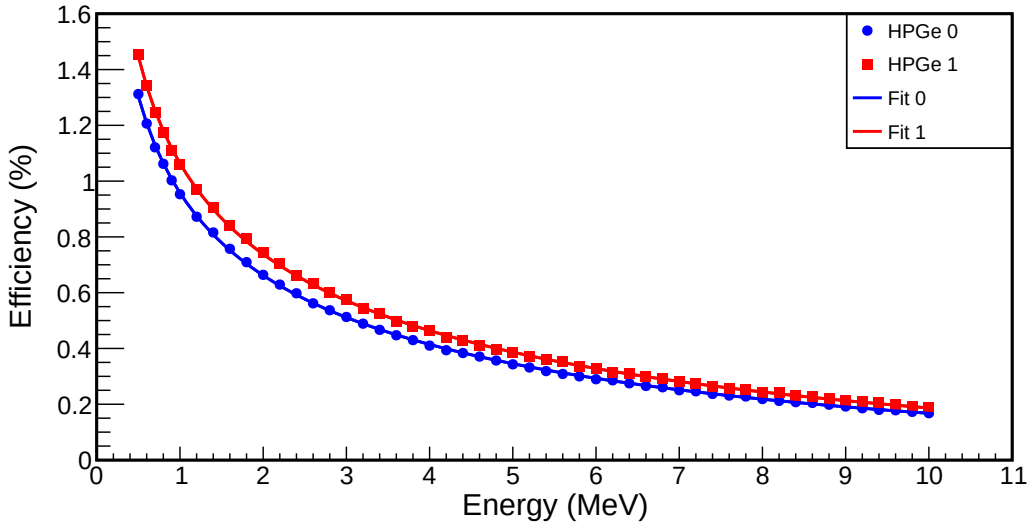


Figure 3. The absolute detection efficiency of the HPGe detectors determined by the Geant4 simulation.

3. Data Analysis and Results

3.1. γ Spectrum

The energy calibration of the HPGe detector was performed using ^{56}Co and ^{152}Eu standard sources, along with the γ rays at 511 keV and from the de-excitation of ^{20}Ne at 8638 and 11,258.9 keV, respectively. The 11,262.3 keV 1^+ state is known with high precision from the ^{16}O$(\alpha, \gamma)^{20}$Ne reaction [37] and the ^{20}Ne(γ, γ') photon scattering [38], the 11,258.9(1.9) keV γ transition is thus used for the energy calibration of the γ single spectrum. The energy-channel relationship of the HPGe detector showed excellent linearity. The calibrated γ-ray data from the two HPGe detectors were summed together, as shown

in Figure 4. The properties of the observed γ rays from the β decay of ^{20}Na are summarized in Table 1.

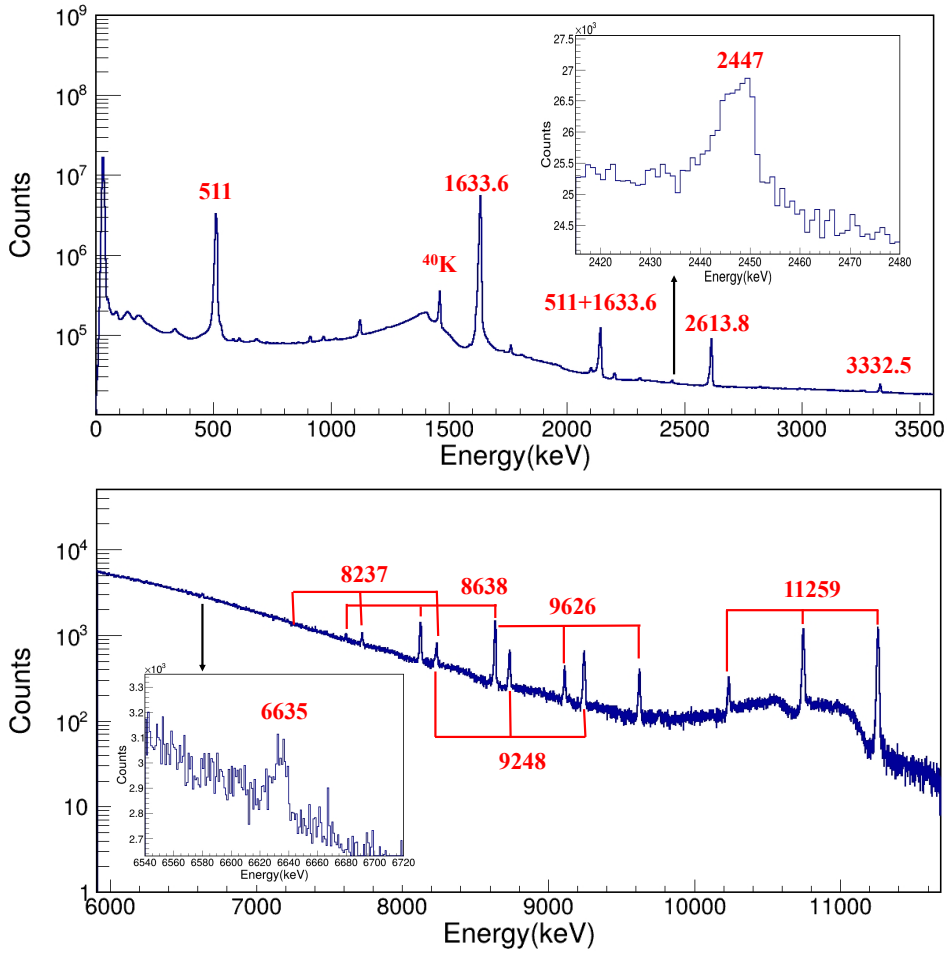


Figure 4. γ singles spectrum of the β decay of ^{20}Na.

Since the decay of ^{20}Na proceeds dominantly to the 1634 keV 2^+_1 and alpha resonance states in ^{20}Ne, only a few known γ lines show up in the γ singles spectrum. In the low-energy part of the γ spectrum, two γ rays were clearly observed: one is at 1633.6 keV, which corresponds to the transition from the 1633.6 keV 2^+_1 level to the $0^+_{\text{g.s.}}$ in ^{20}Ne; the other is at 3332.5 keV, corresponding to the transition from the 4966.5 keV 2^-_1 level to the 1633.6 keV 2^+_1 level. In the high-energy part of the spectrum, five high-energy γ rays were observed at 8237 keV (9873 keV $3^+_1 \rightarrow 2^+_1$), 8638 keV (10,273.2 keV $2^+_6 \rightarrow 2^+_1$) [39], 9248 keV (10,884 keV $3^+_2 \rightarrow 2^+_1$), 9626 keV (11,262.3 keV $1^+_1 \rightarrow 2^+_1$), and 11,258.9 keV (11,262.3 keV $1^+_1 \rightarrow 0^+_{\text{g.s.}}$). For each of these high-energy γ rays, the corresponding single-escape and double-escape peaks were also clearly visible, as labeled in the spectrum. The 10,277 keV IAS, 10,887 and 11,262 keV levels are known to have $T = 1$, the emission of an α particle to the ground state of ^{16}O is isospin forbidden, which results in the enhancement of the emission of γ transitions. Although the 9875 keV 3^+ state has $T = 0$, the emission of an α particle to the ground state of ^{16}O is also forbidden due to its unnatural parity.

Table 1. List of γ rays from the decay of ^{20}Na, with the relative intensities normalized to the 1633.6 keV $2_1^+ \rightarrow 0_{g.s.}^+$ transition. 100 γ intensity units corresponds to a direct β feeding of 79.6(2.5)%.

E_γ(keV)	I_γ(rel.)	E_i(keV)	E_f(keV)	I_i^π	I_f^π
1633.6	100.00(4)	1633.6	0	2_1^+	0_1^+
2440.4	0.0012(1)	10,273.2	7833.4	2_6^+	2_3^+
2451		9873	7421.9	3_1^+	2_2^+
3332.5	0.143(9)	4966.5	1633.6	2_1^-	2_1^+
6635	0.028(6)	10,843	4247.7	2_8^+	4_1^+
8237	0.025(3)	9873	1633.6	3_1^+	2_1^+
8638	0.110(3)	10,273.2	1633.6	2_6^+	2_1^+
9248	0.053(3)	10,884	1633.6	3_2^+	2_1^+
9626	0.032(2)	11,262.3	1633.6	1_1^+	2_1^+
11,258.9	0.162(4)	11,262.3	0	1_1^+	0_1^+

A γ-ray peak at 2613.8 keV was observed in the spectrum, which might be attributed to the transition from the 4247.7 keV 4^+ level to the 1633.6 keV 2_1^+ level in ^{20}Ne. However, this γ peak lies very close to the 2614.5 keV background γ line arising from the ^{208}Bi and ^{208}Tl decay and, therefore, cannot be resolved within the energy resolution of the HPGe detectors. As a result, the origin of this γ ray cannot be unambiguously assigned. A peak observed around 2447 keV is likely composed of contributions from two closely spaced γ rays, i.e., the 2451 keV transition from the 9873 keV 3^+ level to the 7421.9 keV 2^+ level and the 2440.4 keV transition from the 10,273.2 keV 2^+ level to the 7833.4 keV 2^+ level. Owing to their small energy difference, these two transitions could not be clearly resolved in the energy spectrum. Furthermore, a weak peak was observed at around 6635 keV, which may correspond to the transition from the 10,884 keV 3^+ level to the 4247.7 keV 4^+ level. Although the 6635 keV and 2447 keV γ rays form a cascade in the proposed decay scheme, the coincidence relationship cannot be observed due to very weak branchings. The $\gamma - \gamma$ coincidence spectrum gated by the 1634 keV $2_1^+ \rightarrow 0_{g.s.}^+$ transition in ^{20}Ne was also analyzed, which did not exhibit any new γ lines but confirmed the above-discussed γ transitions to the 1634 keV 2_1^+ level.

The relative intensities of the γ rays from the decay of ^{20}Na are listed in Table 1, after being normalized to that of the 1633.6 keV γ line using the simple formula

$$I_\gamma = \frac{N_\gamma / \varepsilon_\gamma}{N_{1633.6} / \varepsilon_{1633.6}} \quad (2)$$

where N_γ and $N_{1633.6}$ are the net counts of the γ ray and the 1633.6 keV, and ε_γ and $\varepsilon_{1633.6}$ are the detection efficiencies at the corresponding energies, respectively.

3.2. α Spectrum

The α energy calibration was based on the two most intense β-delayed α lines of ^{20}Na, at 2153.2(10) keV and 4433.8(15) keV, respectively, with the correction of the energy-loss nonlinearity of the α particle in the aluminum foil and the dead layer of DSSD [26]. Their energies were calculated using the excitation energies of the corresponding states in ^{20}Ne, which are 7421.9(12) keV and 10,273.2(19) keV, along with the α-particle separation energy $S_\alpha = 4729.84(1)$ keV for the decay of $^{20}\text{Ne} \rightarrow {}^{16}\text{O} + \alpha$. The calibrated alpha-particle singles spectrum is shown in Figure 5. Nine α-particle lines are clearly observed in the spectrum,

which are listed in Table 2. Their relative intensities were scaled to the 2153.2 keV α line. The leftmost peak, indicated by a star, corresponds to the recoil ^{16}O.

In the α spectrum obtained in this work, the new low-energy α lines reported by Lauren et al. at 714, 847 and 1220 [26] were not directly observed; these weak α lines were obscured by the ^{16}O recoils. The experimental setup did not offer much opportunity for the ^{16}O and α coincidence, as was applied in Ref. [26]. Instead, we focus on the α-γ coincidence according to the excellent energy resolution of HPGe detectors.

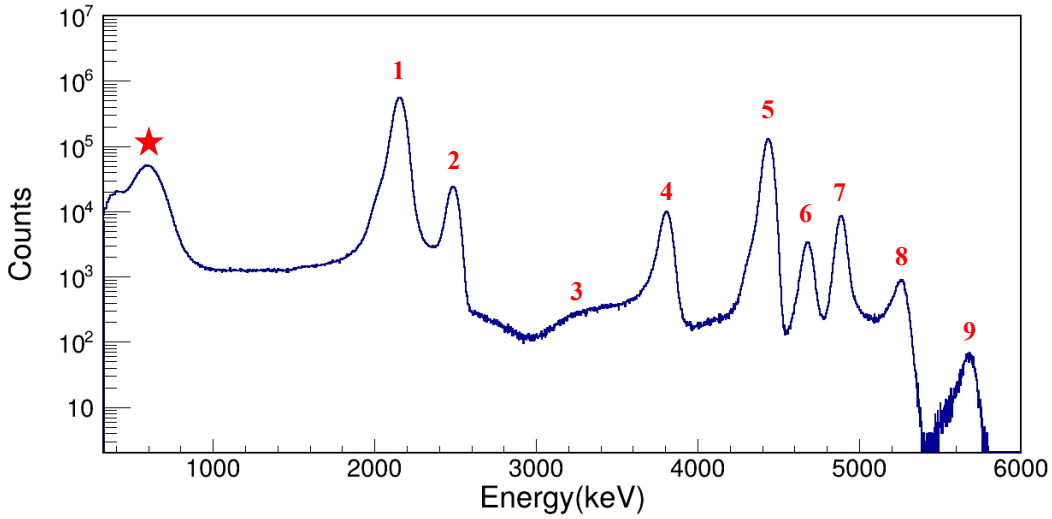


Figure 5. α spectrum from the decay of ^{20}Na. The peak labeled by a star is dominated by ^{16}O recoils.

Table 2. List of α lines from the decay of ^{20}Na, with relative intensities normalized to the 2153.2(10) keV line. 100 α intensity unit corresponds to a direct β of 16.2(0.5)%.

Line	E_α(keV)	I_α(%)	E_i(keV)	I_i^π	I_f^π(^{16}O)
1	2153.2(10)	100.000(252)	7421.9	2_2^+	$0_{g.s.}^+$
2	2486.1(9)	4.305(11)	7833.4	2_3^+	$0_{g.s.}^+$
3	3210(1)	0.232(1)	8767	2_4^+	$0_{g.s.}^+$
4	3806.8(12)	1.929(5)	9487	2_5^+	$0_{g.s.}^+$
5	4433.8(15)	17.255(44)	10,273.2	2_6^+	$0_{g.s.}^+$
6	4680.0(18)	0.531(1)	10,584	2_7^+	$0_{g.s.}^+$
7	4888.1(19)	1.206(3)	10,843	2_8^+	$0_{g.s.}^+$
8	5256.5(26)	0.219(1)	11,320	2_9^+	$0_{g.s.}^+$
9	5678.2(35)	0.014(0)	11,885	2_{10}^+	$0_{g.s.}^+$

The total α particle emission probability, I_α(total), is deduced to be 20.3(6)% from the total α counts N_α(total) by the following relation:

$$I_\alpha(total) = \frac{N_\alpha(total)}{N_\gamma(1634) + N_\gamma(11,259) + N_\alpha(total)}. \quad (3)$$

The intensity of the 1634 keV γ transition is deduced to be 79.6(2.5)% per 100 decays of ^{20}Na from the net counts $N_\gamma(1634)$ by the similar relation

$$I_\gamma(1634) = \frac{N_\gamma(1634)}{N_\gamma(1634) + N_\gamma(11,259) + N_\alpha(total)}. \quad (4)$$

3.3. α-γ Coincidence

To explore the exotic β-γ-α decay sequences of ^{20}Na, an α-γ matrix was constructed that included all α-γ coincidental events within 160 ns, as shown in Figure 6. Since the readout energy of a single α particle event by the front (E_f) and back sides (E_b) of a DSSD is equal, the E_f versus E_b follows a diagonal relation. The fault α-γ coincidence events were removed by introducing a simple criterion, $|E_f - E_b| < 140$ keV. The α-gated γ spectra were projected at different α particle energy intervals from the α-γ matrix, as shown in Figure 7. The ^{16}O recoil events in Figure 5 are related to the α groups by $E(^{16}\mathrm{O}) = 1/4E_\alpha$, and no γ lines are observed in coincidence with the ^{16}O recoils, as is indicated in Figure 7a as an example.

Using α particles in the range of E_a = 640–780 keV as the gate, which corresponds to the α transition from the 3^- state of ^{20}Ne to the 0^+ state of ^{16}O, γ rays with energies of 4252 keV and 4655 keV were observed. These γ rays originate from the de-excitation of the 3^+ state at 9875 keV to the 3^- state at 5621 keV and from the de-excitation of the 2^+ state at 10,277 keV to the same 3^- state at 5621 keV in ^{20}Ne, respectively.

With the use of α particles in the range of E_a = 1520–1640 keV as the gate, corresponding to the known α transition from the 0^+ state at 6720 keV in ^{20}Ne to the ground state of ^{16}O, a γ ray with an energy of 4542 keV was observed. This γ ray results from an M1 transition from the 1^+ state at 11,262 keV in ^{20}Ne to the 0^+ state at 6720 keV. These three coincidence events constitute the β-γ-α decay sequence of ^{20}Na and represent the first experimental observation of this exotic decay mode [27].

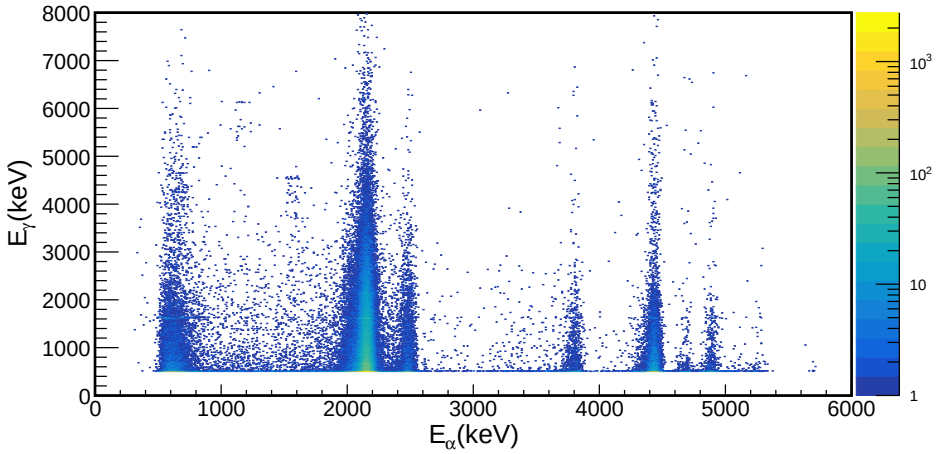


Figure 6. Two-dimensional α-γ coincidence spectrum of ^{20}Na decay.

A γ line at 6130 keV is seen in Figure 7c with an α particle energy gate at E_α = 1110–1240 keV. The 6130 keV γ line is the 6130 keV $3^- \rightarrow 0^+$ transition in ^{16}O; the α particle energy gate indicates a central energy of $E_\alpha = 1175$ keV. Combining this information together reveals that the α-γ coincidence events are attributed to a known 2^+ level at 12,327 keV in ^{20}Ne, which was previously established in high-resolution ^{16}O(α,α) scattering [40]. The new 12,390 keV 1^+ level in ^{20}Ne suggested in Ref. [26] is, therefore, not supported in the present work. No γ line is observed in coincidence with the E_α = 846 keV region, which indicates that the 846 keV α particle intensity observed in Ref. [26] comes from the direct β feeding to the 5788 keV 1^- state in ^{20}Ne.

Gating on the 4252 keV and 4655 keV γ rays, we observed an α particle group with energy of 710(10) keV, consistent with the previously reported value of 714(4) keV in Ref. [26], as shown in Figure 8.

The exotic decay sequences observed in this work by α-γ coincidence are listed in Table 3.

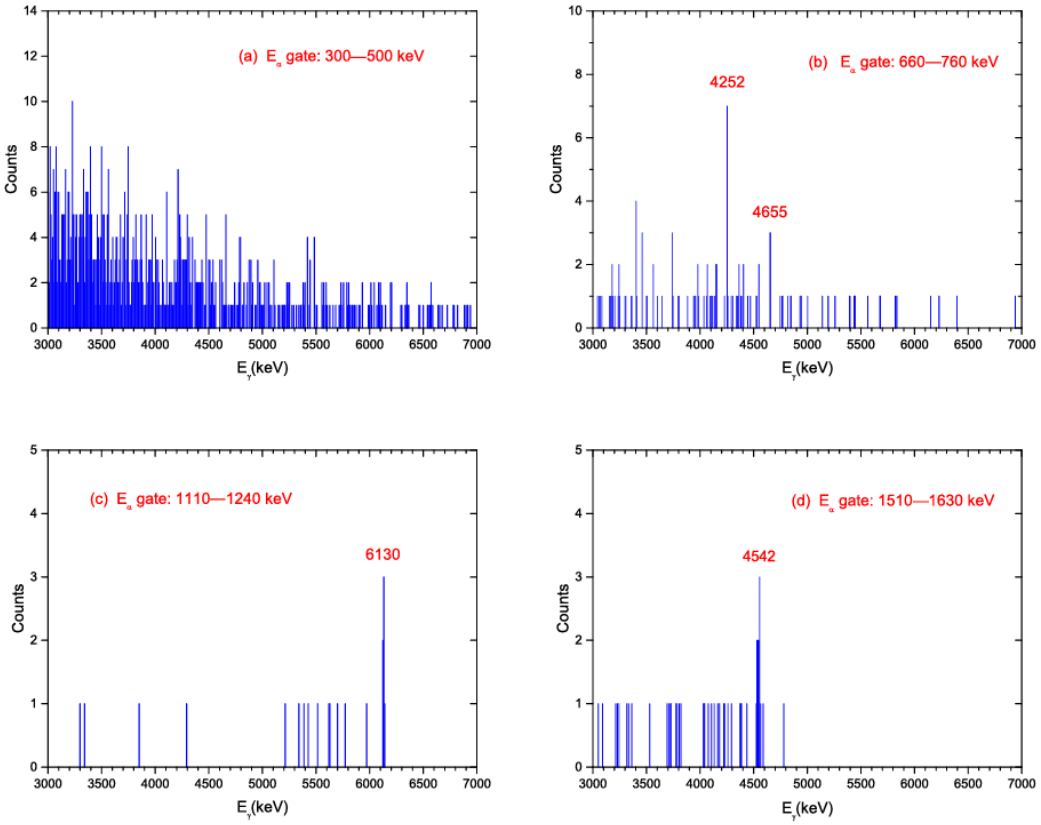


Figure 7. γ spectra projected from the α-γ matrix with different α particle energy gates.

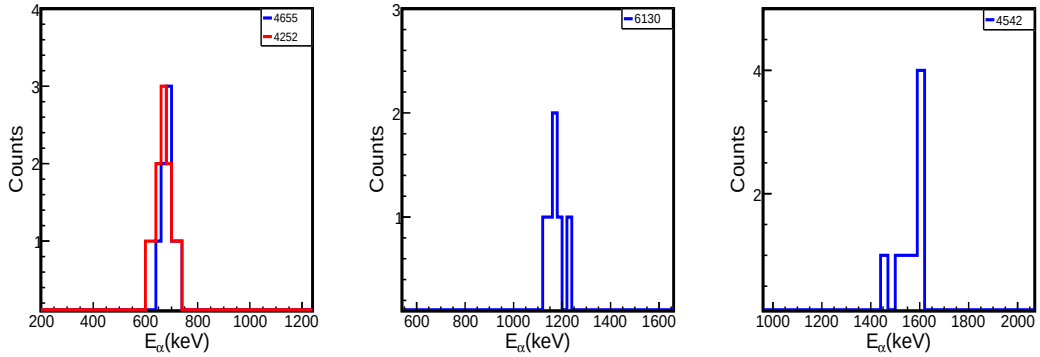


Figure 8. α spectra projected from the α-γ matrix with different γ line energy gates.

Table 3. Exotic decay sequences observed in this work by α-γ coincidence.

E_γ(keV)	E_i(keV)	E_f(keV)	I_i^π	I_f^π	I_γ(%) [1]	E_α(keV)	Decay Sequence
4252(5)	9874.5	5621.4	3^+	3^-	0.0018(6)	710(10)	β-γ-α
4542(5)	11,262.3	6720	1^+	0^+	0.0024(7)	1590(30)	β-γ-α
4655(4)	10,276.7	5621.4	2^+	3^-	0.0016(6)	710(10)	β-γ-α
6130(4)	6130	0	3^+	0^+	0.0016(7)	1204(35)	β-α-γ

[1] Absolute intensity per 100 ^{20}Na decay.

3.4. B(F) and B(GT)

The energy levels of ^{20}Ne populated in the β decay of ^{20}Na are listed in Table 4. The β-feedings to the excited states of ^{20}Ne and the corresponding logft values are calculated by the relative intensities of α, γ and the α-γ coincidence obtained in this work, except for the 5788 keV 1^- state that is taken from Ref. [26]. As one can see from Table 4, for the 1^+, 2^+ and 3^+ states in the daughter nucleus ^{20}Ne, the logft values ranging from 3.8 to

5.9 generally agree with the allowed G-T transitions. For the 10,277 keV IAS in ^{20}Ne in particular, the super-allowed Fermi transition is indicated by a logft value of 3.5. The 8767(30) keV 2^+ state in ^{20}Ne is known to have an α particle width of about 700 keV [26]; it is difficult to evaluate the resonance energy and the α intensity precisely from Figure 5 due to an intense α peak centered at 3810 keV. The B(F) and B(GT) values listed in Table 4 are computed from the experimental logft by the well-known relation [41]

$$ft = \frac{K}{g_V^2 B(F) + g_A^2 B(GT)}, \quad (5)$$

where $K/g_V^2 = 6145(4)$ s, and $g_A/g_V = -1.2670(35)$.

Table 4. The levels of ^{20}Ne populated in the β decay of ^{20}Na. The Logft values are calculated with Q_β = 13,892.5(11) keV [9] and $T_{1/2}$ = 447.9(23) ms [8]. $B_{F/GT}$ indicates the experimentally deduced Fermi or Gamow–Teller transition strengths. The shell model calculation in the *sd*-shell model space is listed for comparison.

		Present Experiment			Shell Model		
E_x (keV)	I^π	β-Feeding (%)	logft	$B_{F/GT}$	E_x (keV)	B_{GT} [a]	B (F)
0.0	0^+						
1633.7 (2) [b]	2^+	79.3(25)	4.99	0.039	1738	0.035	0.00001
4968.0 (7) [b]	2^-	0.114(8)	7.10				
5621.4 (17) [c]	3^-	<0.0029	>8.5				
5787.7 (26) [c]	1^-	0.0016(5) [d]	8.73				
6720 (5) [b]	0^+				6698		
7423.5 (18)	2^+	16.1(6)	4.19	0.245	7533	0.182	0.00044
7831.8 (23)	2^+	0.69(3)	5.40	0.015			
8770 (50)	2^+	0.034(8)	6.30	0.002			
9488.5 (22)	2^+	0.307(18)	4.96	0.042			
9874.5 (21) [b]	3^+	0.022(6)	5.87	0.005	10,419	0.0005	
10,276.7 (20) [b]	2^+	2.87(12)	3.48	2.044	9947	0.093	1.994
10,582 (3)	2^+	0.085(4)	4.77	0.065	10,440	0.201	0.0024
10,841.5 (22)	2^+	0.195(8)	4.18	0.253	10,747	0.417	0.0025
10,886.8 (22) [b]	3^+	0.042(4)	4.80	0.060	10,538	0.086	
11,262.3 (19) [b]	1^+	0.157(8)	3.84	0.552	11,135	0.510	
11,300 (10)	2^+	0.035(2)	4.45	0.135			
11,870 (50)	2^+	0.0023(1)	4.81	0.059			
12,367 (35)	1^+	0.0016(7)	3.82	0.577	12,573	0.211	

[a] A quenching factor of $q^2_{(GT)} = 0.60$ [42] is multiplied. [b] Determined by γ transitions from this work. The remaining excitation energies are determined by α particle lines or otherwise labeled. [c] From compilation in Ref. [39]. [d] From Ref. [26].

The β decay of ^{20}Na is calculated in the *sd*-shell model space with a USDB interaction [43] for the charge-independent part plus the Coulomb, charge-dependent and charge-asymmetric nuclear Hamiltonian obtained by Ormand and Brown for the *sd* shell [44]. As listed in Table 4, five 2^+ states and one 1^+ state in ^{20}Ne are predicted with β transition strengths from the ^{20}Na decay, and the calculated B(GT) values scaled with a typical quenching factor of 0.6 agree well with the experimental ones. For the 10,277 keV IAS in ^{20}Ne, the calculated total β transition strength includes about 3% of $B(GT)$ mixing to

the $B(F)$ of 2.0. Three 3^+ states in ^{20}Ne are predicted within the excitation energies from 10.5 to 11.6 MeV, and the shell model 3^+_2 state agrees very well with the experimental one in terms of the excitation energy and B(GT) value. For the 3^+_2 state in ^{20}Ne, the experimental B(GT) value is only less than one-quarter of the shell model prediction; the discrepancy arises from the predicted strong $E2$ γ transitions to the low-lying 2^+_2 and 4^+_1 states that were not observed in this work. Another 3^+_3 state is predicted at 11.611 MeV in ^{20}Ne with a weak β branching of about 0.0016%, which has not been observed in the decay of ^{20}Na to date. We notice that the lowest excitation levels in ^{19}F are probably single-valence proton excitation from $2s_{1/2}$ to $1p_{1/2}$ and $1d_{5/2}$, as well as single-valence neutron excitation from $2s_{1/2}$ to $1d_{5/2}$ and $1p_{1/2}$ in ^{19}Ne; the main configurations for the lowest 2^- and 3^- levels in ^{20}Ne may involve $\pi 1p_{1/2} \oplus \nu 1d_{5/2}$ and $\pi 1d_{5/2} \oplus \nu 1p_{1/2}$. Naively, the lowest 1^- and 4^- levels in ^{20}Ne could have originated from the coupling of the proton and neutron $1d_{5/2}$ and $1p_{3/2}$ single-particle orbitals. A shell-model calculation in the *psd*–shell model space with a YSOX interaction [45] indeed predicts the 2^- and 3^- states in ^{20}Ne at reasonable excitation energies of 7696 and 7941 keV, respectively.

3.5. Decay Scheme

A decay scheme of ^{20}Na is shown in Figure 9. Three β-γ-α decay sequences and one β-α-γ exotic decay sequence in ^{20}Na that were observed in the present work are marked in red in Figure 9.

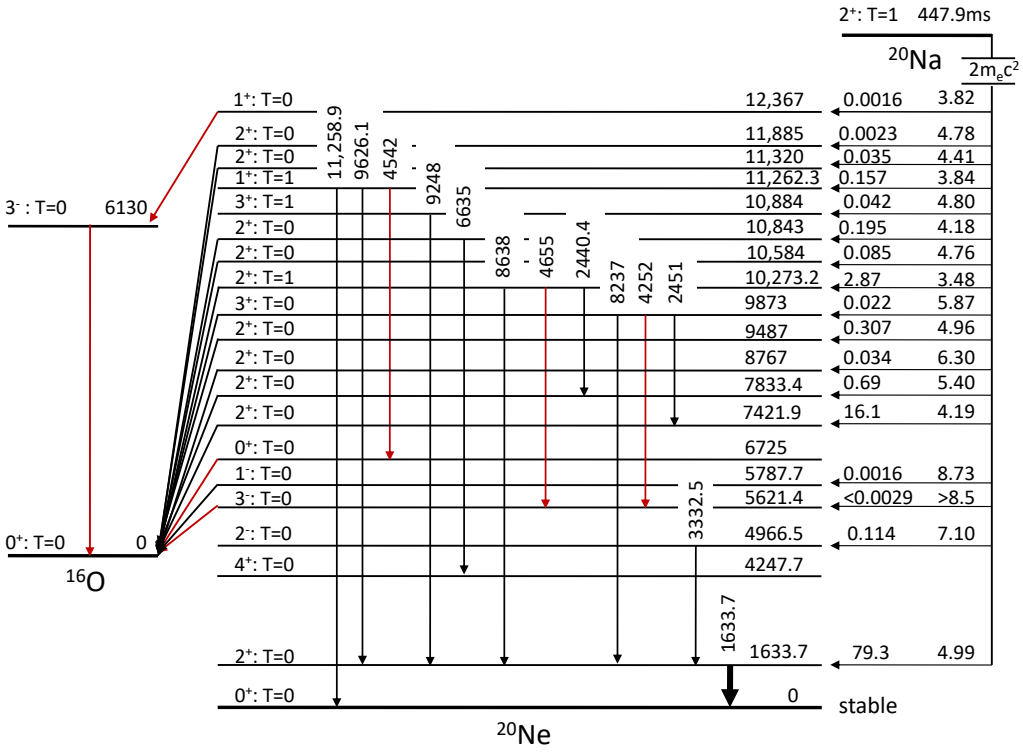


Figure 9. Decay scheme of ^{20}Na. The newly discovered exotic decay sequences are shown with red arrows. The ^{20}Ne states are labeled by excitation energy in keV, the β branching ratio, and the logft value on the right side.

The 4252 keV and 4655 keV γ rays contribute to the intensity of the 714 keV α particle. This occurs because the 3^-, T = 0, state of ^{20}Ne at 5621 keV is populated by a first-forbidden beta transition (Logft > 8.5) from ^{20}Na, while the 3^+, T = 0 state at 9874.5 keV, which emits the 4252 keV γ ray, and the 2^+, T = 1 state at 10,277 keV, which emits the 4655 keV γ ray, are populated by allowed beta transitions from ^{20}Na with Logft values of 5.87 and 3.48, respectively. Both γ rays correspond to E1 transitions. Notably, the 2^+, T = 1 state

at 10,277 keV can decay by α particle emission only by mixing with nearby 2^+ states with $T = 0$. The intensity of the 1589 keV α particle comes dominantly from 4542 keV γ ray indirect feeding, instead of the second-forbidden direct β transition. The 1220 keV α particle line originates from the decay of the 12,367 keV excited state in ^{20}Ne to the 6130 keV state in ^{16}O. With a Logft value of 3.82, this transition is classified as allowed. An angular distribution analysis from the ^{19}F(^{3}He,d)^{20}Ne reaction determines the spin-parity of this state as 1^+. Given that the 3^- state of ^{16}O has an isospin values of T = 0, the 12,367 keV state is consequently assigned an isospin of T = 0.

4. Summary

In summary, the β decay of ^{20}Na was investigated in the day-one experiment at BRIF with an intense, pure ^{20}Na ISOL beam and a challenging α–γ coincidence analysis. Three exotic β–γ–α decay sequences in ^{20}Na were successfully observed, comprising the first case of its type and, thus, expanding the rare decay modes discovered in β decay. The observed β–γ–α decay sequences are essential in determining the direct β feedings and log ft values for the low-lying α-emitting states in ^{20}Ne. Although the α decay widths for these states have not been calculated, the experimental β transition strengths for the 1^+, 2^+, and 3^+ states in ^{20}Ne can be well accounted for using sd shell-model space interactions. It is clear that the low-lying negative parity states in ^{20}Ne involve $1p$, instead of a $1f$ single-particle orbital; however, the complexity of cross-shell excitation limits the precision of the predictions for these negative parity states in ^{20}Ne from a shell-model calculation in the *psd*-shell space.

Author Contributions: Conceptualization, Q.W., Y.-B.W., J.S., S.Z., Z.-H.L., B.G., and W.-P.L.; methodology, Q.W., Y.-B.W., J.S., Z.-Y.H., Y.-J.L., X.-Y.L., S.-Q.Y., G.L., Y.-P.S., and B.A.B.; software, Q.W.; validation, Y.-B.W.; formal analysis, Q.W. and Y.-B.W.; investigation, Q.W., Y.-B.W., and Z.-Y.H.; resources, L.-H.C., Z.-Q.C., B.-Q.C., B.D., T.G., Y.-L.L., R.-G.M., X.M., Y.-J.M., Y.S., B.T., C.-G.W., H.-Y.W., F.-R.X., Y.Z., C.Z., and T.-J.Z.; data curation, Q.W., H.Z., and T.-L.M.; writing—original draft preparation, Q.W. and Y.-B.W.; writing—review and editing, Q.W. and Y.-B.W.; visualization, Q.W.; supervision, Y.-B.W.; project administration, Y.-B.W.; funding acquisition, Y.-B.W. All authors have read and agreed to the published version of the manuscript.

Funding: Supported by the National Key Research and Development Project under Grant No. 2022YFA1602301, the National Natural Science Foundation of China under Grants Nos. U2267205 and 12275361, and the Continuous-Support Basic Scientific Research Project. B.A.B. was supported by the United States National Science Foundation grant PHY-2110365.

Data Availability Statement: The data is not publicly available due to technical reasons (a huge data volume); in part, it may be obtained from the authors upon request.

Acknowledgments: The authors are grateful to the administrative and technical staff at the BRIF laboratory for their invaluable assistance.

Conflicts of Interest: The authors declare no conflicts of interest.

References

1. Tanihata, I.; Hamagaki, H.; Hashimoto, O.; Shida, Y.; Yoshikawa, N.; Sugimoto, K.; Yamakawa, O.; Kobayashi, T.; Takahashi, N. Measurements of Interaction Cross Sections and Nuclear Radii in the Light p- Shell Region. *Phys. Rev. Lett.* **1985**, *55*, 2676–2679. [CrossRef]
2. Glassman, B.E.; Pérez-Loureiro, D.; Wrede, C.; Allen, J.; Bardayan, D.W.; Bennett, M.B.; Brown, B.A.; Chipps, K.A.; Febbraro, M.; Fry, C.; et al. Revalidation of the isobaric multiplet mass equation for the A = 20 quintet. *Phys. Rev. C* **2015**, *92*, 042501. [CrossRef]
3. Langanke, K.; Martínez-Pinedo, G. Nuclear weak-interaction processes in stars. *Rev. Mod. Phys.* **2003**, *75*, 819–862. [CrossRef]
4. Steppenbeck, D.; Takeuchi, S.; Aoi, N.; Doornenbal, P.; Matsushita, M.; Wang, H.; Baba, H.; Fukuda, N.; Go, S.; Honma, M.; et al. Evidence for a new nuclear 'magic number' from the level structure of 54Ca. *Nature* **2013**, *502*, 207–210. [CrossRef]

5. Giovinazzo, J.; Blank, B.; Borcea, C.; Canchel, G.; Dalouzy, J.C.; Demonchy, C.E.; De Oliveira Santos, F.; Dossat, C.; Grévy, S.; Hay, L.; et al. First Direct Observation of Two Protons in the Decay of Fe 45 with a Time-Projection Chamber. *Phys. Rev. Lett.* **2007**, *99*, 102501. [CrossRef] [PubMed]
6. Yang, L.; Lin, C.J.; Yamaguchi, H.; Moro, A.M.; Ma, N.R.; Wang, D.X.; Cook, K.J.; Mazzocco, M.; Wen, P.W.; Hayakawa, S.; et al. Breakup of the proton halo nucleus 8B near barrier energies. *Nat. Commun.* **2022**, *13*, 7193. [CrossRef]
7. Ye, Y.; Yang, X.; Sakurai, H.; Hu, B. Physics of exotic nuclei. *Nat. Rev. Phys.* **2024**, *7*, 21–37. [CrossRef]
8. Audi, G.; Kondev, F.G.; Wang, M.; Huang, W.; Naimi, S. The NUBASE2016 evaluation of nuclear properties. *Chin. Phys. C* **2017**, *41*, 030001. [CrossRef]
9. Wang, M.; Audi, G.; Kondev, F.G.; Huang, W.; Naimi, S.; Xu, X. The AME2016 atomic mass evaluation (II). Tables, graphs and references. *Chin. Phys. C* **2017**, *41*, 030003. [CrossRef]
10. Firestone, R.B. *Table of Isotopes*; John Wiley: Hoboken, NJ, USA, 1996; Volume 1.0.
11. Costantini, H.; deBoer, R.J.; Azuma, R.E.; Couder, M.; Görres, J.; Hammer, J.W.; LeBlanc, P.J.; Lee, H.Y.; O'Brien, S.; Palumbo, A.; et al. $^{16}O(\alpha,\gamma)^{20}Ne$ S factor: Measurements and R -matrix analysis. *Phys. Rev. C* **2010**, *82*, 035802. [CrossRef]
12. Thielemann, F.K.; Arnett, W.D. Hydrostatic nucleosynthesis. II. Core neon to silicon burning and presupernova abundance yields of massive stars. *Astrophys. J.* **1985**, *295*, 604–619. [CrossRef]
13. Hager, U.; Brown, J.R.; Buchmann, L.; Carmona-Gallardo, M.; Erikson, L.; Fallis, J.; Greife, U.; Hutcheon, D.; Ottewell, D.; Ruiz, C.; et al. Direct total cross section measurement of the 16 O(α,γ) 20 Ne reaction at $E_{c.m.}$ = 2.26 MeV. *Phys. Rev. C* **2011**, *84*, 022801. [CrossRef]
14. Hager, U.; Buchmann, L.; Davids, B.; Fallis, J.; Greife, U.; Hutcheon, D.A.; Irvine, D.; Ottewell, D.; Rojas, A.; Reeve, S.; et al. Direct measurement of the 16 O(α,γ) 20 Ne reaction at $E_{c.m.}$= 2.43 MeV and 1.69 MeV. *Phys. Rev. C* **2012**, *86*, 055802. [CrossRef]
15. Huang, W.X.; Xu, X.J.; Ma, R.C.; Hu, Z.Q.; Guo, J.S.; Guo, Y.X.; Liu, H.Y.; Xu, L.L. Decay study of ^{20}Na and its beta-delayed ^{16}O recoiling. *Sci. China Ser. A Math.* **1997**, *40*, 638–643. [CrossRef]
16. Orrigo, S.; Rubio, B.; Fujita, Y.; Blank, B.; Gelletly, W.; Agramunt, J.; Algora, A.; Ascher, P.; Bilgier, B.; Cáceres, L.; et al. Observation of the β-Delayed γ-Proton Decay of Zn 56 and its Impact on the Gamow-Teller Strength Evaluation. *Phys. Rev. Lett.* **2014**, *112*, 222501. [CrossRef]
17. Bhattacharya, M.; Melconian, D.; Komives, A.; Triambak, S.; García, A.; Adelberger, E.G.; Brown, B.A.; Cooper, M.W.; Glasmacher, T.; Guimaraes, V.; et al. ft value of the $0+ \rightarrow 0+ \beta+$ decay of Ar 32: A measurement of isospin symmetry breaking in a superallowed decay. *Phys. Rev. C* **2008**, *77*, 065503. [CrossRef]
18. Pfützner, M.; Karny, M.; Grigorenko, L.V.; Riisager, K. Radioactive decays at limits of nuclear stability. *Rev. Mod. Phys.* **2012**, *84*, 567–619. [CrossRef]
19. Macfarlane, R.; Siivola, A. Isobaric spin non-conservation in the delayed alpha decay of Na20. *Nucl. Phys.* **1964**, *59*, 168–176. [CrossRef]
20. Pearson, J.D.; Almqvist, E.; Kuehner, J.A. LEVELS IN Ne^{20} FROM THE C^{12} (C^{12} , α)Ne^{20} REACTION. *Can. J. Phys.* **1964**, *42*, 489–493. [CrossRef]
21. Betts, R.R.; Fortune, H.T.; Middleton, R. Structure of ^{20}Ne:The $^{19}F(^3He,d)^{20}Ne$ reaction. *Phys. Rev. C* **1975**, *11*, 19–28. [CrossRef]
22. Ingalls, P.D. Decay of ^{20}Na to γ-ray emitting states of ^{20}Ne. *Phys. Rev. C* **1976**, *14*, 254–260. [CrossRef]
23. Minamisono, K.; Nagatomo, T.; Matsuta, K.; Levy, C.D.P.; Tagishi, Y.; Ogura, M.; Yamaguchi, M.; Ota, H.; Behr, J.A.; Jackson, K.P.; et al. Low-energy test of second-class current in β decays of spin-aligned ^{20}F and ^{20}Na. *Phys. Rev. C* **2011**, *84*, 055501. [CrossRef]
24. Torgerson, D.F.; Wien, K.; Fares, Y.; Oakey, N.S.; Macfarlane, R.D.; Lanford, W.A. $\beta+$ Decay of Na 20. *Phys. Rev. C* **1973**, *8*, 161–167. [CrossRef]
25. Clifford, E.; Hagberg, E.; Hardy, J.; Schmeing, H.; Azuma, R.; Evans, H.; Koslowsky, V.; Schrewe, U.; Sharma, K.; Towner, I. The decay of 20Na: Measurements of isospin mixing and the weak vector coupling constant as well as other new decay data. *Nucl. Phys. A* **1989**, *493*, 293–322. [CrossRef]
26. Laursen, K.L.; Kirsebom, O.S.; Fynbo, H.O.U.; Jokinen, A.; Madurga, M.; Riisager, K.; Saastamoinen, A.; Tengblad, O.; Äystö, J. High-statistics measurement of the β-delayed γ spectrum of ^{20}Na. *Eur. Phys. J. A* **2013**, *49*, 79. [CrossRef]
27. Wang, Y.B.; Su, J.; Han, Z.Y.; Tang, B.; Cui, B.Q.; Ge, T.; Lyu, Y.L.; Brown, B.A.; Yuan, C.X.; Chen, L.H.; et al. Direct observation of the exotic β-γ-α decay mode in the $T_z = -1$ nucleus ^{20}Na. *Phys. Rev. C* **2021**, *103*, L011301. [CrossRef]
28. Guo, B.; Liu, W. Beijing radioactive ion facility and basic nuclear physics research prospects. *Chin. Sci. Bull.* **2015**, *60*, 1820–1827. [CrossRef]
29. Nan, W.; Guo, B.; Chen, J.; Cui, B.; Fu, W.; Jia, X.; Kan, C.; Li, J.; Li, Y.; Lin, C.; et al. Nuclear physics at BRIF. *Prog. Part. Nucl. Phys.* **2025**, *145*, 104188. [CrossRef]
30. Liu, W.; Li, Z.; Bai, X.; Wang, Y.; Guo, B.; Peng, C.; Yang, Y.; Su, J.; Cui, B.; Zhou, S.; et al. BRIF and CARIF progress. *Sci. China Phys. Mech. Astron.* **2011**, *54*, 14–17. [CrossRef]
31. Zhang, T.; Li, Z.; Yin, Z. Design & construction status of CYCIAE-100, a 100 MeV H^- cyclotron for RIB production. *Nucl. Instruments Methods Phys. Res. Sect. B Beam Interact. Mater. Atoms* **2008**, *266*, 4117–4122. [CrossRef]

32. Zhang, T.J.; Guan, X.L.; Cui, B.Q. Design and construction progress of BRIF. *Chin. Phys. C* **2010**, *34*, 103–111. [CrossRef]
33. Tang, B.; Cui, B.; Chen, L.; Huang, Q.; Ma, R.; Ma, Y.; Ma, X.; Jiang, W. The development of the FEBIAD ion source for BRISOL. *Nucl. Instruments Methods Phys. Res. Sect. B Beam Interact. Mater. Atoms* **2020**, *463*, 154–157. [CrossRef]
34. Dombsky, M.; Achtzehn, T.; Bricault, P.; Hackman, G.; Hanemaayer, V.; Lassen, J.; Lavoie, J.; Morton, A.; Pearson, M.; Prime, E.; et al. Development of a high intensity 26gAl beam from SiC targets for accelerated beam experiments at ISAC. *Nucl. Instruments Methods Phys. Res. Sect. B Beam Interact. Mater. Atoms* **2007**, *264*, 117–124. [CrossRef]
35. Nan, W.; Guo, B.; Lin, C.J.; Pang, D.Y.; Yang, L.; Wang, D.X.; Yang, G.; Shen, Y.P.; Tang, B.; Fan, Q.W.; et al. First experiment using post-accelerated unstable ion beams at BRIF: angular distribution of the 21, 22 Na elastic scattering from doubly magic 40 Ca. *Sci. Bull.* **2025**, *70*, 2925–2928. [CrossRef] [PubMed]
36. Meyer, M.; Venter, I.; Reitmann, D. Energy levels of 28Si. *Nucl. Phys. A* **1975**, *250*, 235–256. [CrossRef]
37. Fifield, L.; Catford, W.; Chew, S.; Garman, E.; Pringle, D.; Allen, K.; Lowe, J. Evidence for isovector parity mixing in the 11.264 MeV 1+ T = 1 state in 20Ne. *Nucl. Phys. A* **1983**, *394*, 1–15. [CrossRef]
38. Berg, U.E.P.; Ackermann, K.; Bangert, K.; Stock, R.; Wienhard, K. 11,262 keV 1 + state in Ne 20. *Phys. Rev. C* **1983**, *27*, 2981–2983. [CrossRef]
39. Tilley, D.; Cheves, C.; Kelley, J.; Raman, S.; Weller, H. Energy levels of light nuclei, A = 20. *Nucl. Phys. A* **1998**, *636*, 249–364. [CrossRef]
40. Caskey, G. Natural parity states of Ne 20 for $12 < E_x < 15.5$ MeV. *Phys. Rev. C* **1985**, *31*, 717–735. [CrossRef]
41. Jonson, B.; Riisager, K. Beta-decay of exotic nuclei. *Nucl. Phys. A* **2001**, *693*, 77–89. [CrossRef]
42. Richter, W.A.; Mkhize, S.; Brown, B.A. *sd*-shell observables for the USDA and USDB Hamiltonians. *Phys. Rev. C* **2008**, *78*, 064302. [CrossRef]
43. Brown, B.A.; Richter, W.A. New "USD" Hamiltonians for the sd shell. *Phys. Rev. C* **2006**, *74*, 034315. [CrossRef]
44. Ormand, W.; Brown, B. Empirical isospin-nonconserving hamiltonians for shell-model calculations. *Nucl. Phys. A* **1989**, *491*, 1–23. [CrossRef]
45. Yuan, C.; Suzuki, T.; Otsuka, T.; Xu, F.; Tsunoda, N. Shell-model study of boron, carbon, nitrogen, and oxygen isotopes with a monopole-based universal interaction. *Phys. Rev. C* **2012**, *85*, 064324. [CrossRef]

Disclaimer/Publisher's Note: The statements, opinions and data contained in all publications are solely those of the individual author(s) and contributor(s) and not of MDPI and/or the editor(s). MDPI and/or the editor(s) disclaim responsibility for any injury to people or property resulting from any ideas, methods, instructions or products referred to in the content.